

Photoemission study of the Si(111)3×1-K surface

K. Sakamoto, T. Okuda, H. Nishimoto, H. Daimon, and S. Suga

Department of Material Physics, Faculty of Engineering Science, Osaka University, Toyonaka, Osaka 560, Japan

T. Kinoshita and A. Kakizaki

Tsukuba Branch of Synchrotron Radiation Laboratory, Institute for Solid State Physics,

The University of Tokyo in KEK, Oho, Tsukuba 305, Japan

(Received 12 July 1993; revised manuscript received 24 January 1994)

Surface electronic states of the Si(111)3×1-K surface are studied by means of angle-resolved ultraviolet photoelectron spectroscopy along the $[11\bar{2}]$ and the $[10\bar{1}]$ directions. It is found that the S_1 state (~ 0.2 eV below the Fermi level) of the 7×7 surface disappears and surface states S'_2 and S'_3 appear near the binding energy of ~ 0.9 and ~ 1.8 eV below the Fermi level in the spectra of the Si(111)(3×1)-K surface. Hence, the Si(111)3×1-K surface is no longer metallic like the Si(111)7×7 clean surface but is semiconducting. The saturation coverage of K on the Si(111)3×1-K surface is estimated to be $\frac{1}{3}$ ML from comparison of the Si L_{VV} Auger spectrum and the K $2p$ x-ray-photoemission-spectroscopy peak intensity ratio to that of the Si(111)87×7-K surface. From these results, we suggest a surface geometrical structural model for the Si(111)3×1-K surface.

INTRODUCTION

Studies of alkali-metal adsorption on semiconductor surfaces are very interesting subjects with respect to the changes of the geometrical and electronic structures. Among these, the Si(001)-K and Si(111)-K systems have been studied most extensively.¹⁻⁷ The structural changes of the Si(111)7×7 surface by alkali-metal adsorption have been observed by means of reflection high-energy electron diffraction (RHEED),^{5,8} low-energy electron diffraction (LEED),⁹⁻¹¹ scanning tunneling microscope (STM),^{6,12,13} Auger electron spectroscopy,¹¹ scanning tunneling spectroscopy (STS),¹³ ion scattering spectroscopy (ISS),⁷ and core-level shift.¹⁴ Daimon and Ino⁵ found another 7×7 structure at room temperature, named 87×7 , and a 3×1 structure at high temperature for all alkali metals (Li, Na, K, Rb, and Cs) using RHEED, and proposed the saturation coverage of the 3×1 surface as $\frac{2}{3}$ ML. Mizuno and Ichimiya⁸ heated the Si(111)1×1-Li surface and found 4×4 , $\sqrt{3}\times\sqrt{3}$, and 3×1 RHEED patterns with increasing temperature (this condition corresponds to a decrease of the coverage). LEED studies⁹⁻¹¹ have pointed out that these 3×1 surfaces show very similar intensity-voltage (I - V) curves suggesting that the 3×1 phase is made of Si reconstruction only being stabilized by a small amount of alkali metals. Fan and Ignatiev¹¹ studied the Li- and Na-covered Si(111) surfaces at 0.01 ML, and found the 3×1 reconstructed surface even at this coverage. Hashizume *et al.*⁶ observed the Si(111)3×1-K structure at 300 °C using field-ion STM, and proposed a structural model, which has two K atoms in the 3×1 unit mesh. Wan, Lin, and Nogami¹² studied the 3×1 reconstruction of the Si(111) surface induced by adsorption of Li using STM, and proposed a missing-top-layer model which has parallel “ π -bond-like” chains of which the Si atoms are terminated by the Li atoms, and one dangling bond per unit

cell remains. The number of Li atoms in the 3×1 unit mesh is two. Recently, Hashizume *et al.*⁷ measured the absolute K coverage of the Si(111)3×1-K surface by ISS as $\frac{1}{3}$ ML. Okuda *et al.*¹⁴ also suggested the saturation coverage of the Si(111)3×1-Na surface as $\frac{1}{3}$ ML. In this way, the structural model and the saturation coverage of these alkali-metal-adsorbed 3×1 surfaces are still controversial problems.

The electronic structure of alkali-metal-adsorbed Si(111) surfaces at room temperature has been studied experimentally using ultraviolet photoemission spectroscopy (UPS),^{15,16} angle-resolved UPS (ARUPS),¹⁷ and inverse photoemission spectroscopy.¹⁶ Magnusson and Reihl¹⁶ have observed the changes of the occupied surface states S_1 , S_2 , and S_3 , and that of the unoccupied surface state U_1 (0.5 eV above the Fermi level), which is the adatom-derived empty surface state, upon evaporation of K. Namely, the S_1 state shifted to larger E_B from the Fermi level with increasing intensity in the initial stage of the K adsorption, and the Fermi-level crossing disappeared. S_2 and S_3 states also shifted to larger E_B , but after a certain evaporation time, the intensity of the S_3 state became weak and the S_2 structure merged with the S_1 structure. (The same results are independently confirmed by Tezuka, Daimon, and Ino.¹⁷) Although the intensity of the empty surface state U_1 drastically decreased and vanished after a certain evaporation time, an empty surface state U'_1 appeared at 1.0 eV above the Fermi level. They concluded that the K atoms adsorbed on the dangling bonds made the Si(111)87×7-K surface semiconducting. Based on their result, the saturation coverage of the Si(111)87×7-K surface will be more than $\frac{19}{49}$, when there are more than one K atom per (average) Si(111) dangling bond. Jeon *et al.*¹³ measured the I - V curves of the Si(111)3×1-Na surface with STS, and found the surface-state band gap of about 1 eV.

The π -bonded chain model is the cornerstone of our structural model. Pandey¹⁸ proposed the π -bonded chain model for the Si(111)2 \times 1 cleaved surface and calculated the energy of the surface-state bands. Here, the surface Si atoms constitute seven-membered and five-membered rings, and the dangling bonds on the seven-membered rings are π bonded and make one-dimensional chains along the [10 $\bar{1}$] direction. The dispersions of these surface states have been measured using ARUPS by Uhrberg *et al.*¹⁹ The dispersions calculated by Northrup and Cohen²⁰ are in good agreement with the experimental data of Uhrberg *et al.*, but are a little different from those of Pandey. The main difference between these two theoretical results is the existence of an extremum of dispersion between the $\bar{\Gamma}$ and \bar{J} points in the model of Northrup and Cohen in contrast to no extremum in Pandey's model. The predicted dispersion of the π -bonded chain along the $\bar{\Gamma}$ - \bar{J} and \bar{J} - \bar{K}' directions, calculated by Northrup and Cohen, are ~ 0.8 and ~ 0.08 eV, with the smallest E_B situated at the \bar{K}' point (\bar{J} and \bar{K}' are the symmetry points of the 2 \times 1 surface).²⁰ Ignoring the extremum of the dispersion, i.e., considering only the difference of E_B at the $\bar{\Gamma}$ and \bar{K}' points, the difference is 0.57 eV. On the other hand, the width of the dispersion calculated by Pandey is almost the same (0.58 eV). Due to the one-dimensional π -bonded chain, this surface is in principle a quasi-one-dimensional metal, but practically some distortion can induce a band gap and a semiconducting surface character.

EXPERIMENT

The experiments were performed at the beam line BL-18A of Photon Factory installed by the Institute for Solid State Physics of the University of Tokyo in collaboration with the National Laboratory for High Energy Physics (KEK). This beam line is equipped with a constant-deviation-angle grazing-incidence monochromator and an angle-resolved photoelectron spectrometer (VG ADES 500). The overall instrumental angular and energy resolutions were $\sim 1^\circ$ and ~ 150 meV, respectively, at $h\nu=21.2$ eV. The analyzer chamber was also equipped with a LEED system, a Mg/Al twin anode x-ray source, and an electron spectrometer (VG CLAM) for x-ray-photoemission spectroscopy (XPS). The base pressure of this chamber was 2×10^{-11} Torr.

The sample was a P-doped Si wafer with the electrical resistivity of 2.4–4.0 Ω cm and the size of 4 \times 20 \times 0.6 mm³. The clean surface was obtained by direct-current heating up to $\sim 1250^\circ\text{C}$ (five times for 3 sec) in the UHV chamber. The surface quality and the cleanliness were checked by the observation of the 7 \times 7 LEED pattern and the lack of the peak of the O 1s and C 1s signals in the XPS spectra.

In order to make a Si(111)8 \times 7-K structure, the Si wafer was spontaneously cooled down for several minutes after flashing up to 1250 $^\circ\text{C}$. The K atoms were then deposited using an alkali-metal dispenser (from SAES Getters), which was mounted about 3 cm apart from the Si wafer. On the other hand, the Si wafer was kept at 500 $^\circ\text{C}$ during the deposition in order to make a good

Si(111)3 \times 1-K structure.⁵ The pressure during the K deposition was close to 1.5×10^{-10} Torr. We checked the amount of adsorption of the K atoms by the change of the LEED pattern and the change of the work function from the value of the clean surface, 4.595 eV. The determination of the saturation coverage was made by measuring the change of work function and the ratio of the XPS intensities of the Si LVV Auger peak and the K 2p core XPS peak.

RESULTS AND DISCUSSION

The UPS spectra taken for the Si(111)7 \times 7 clean surface and the Si(111)3 \times 1-K surface at the emission angle $\theta_e=0\pm 0.5^\circ$ (surface normal) are shown in Fig. 1. The incidence angle θ_i of the linear polarized light (p polarized) was 45° from the surface normal. The accurate surface-normal direction was determined from the symmetry of the observed dispersion. The Fermi-level position in the UPS spectra was determined from the measurement of the metallic Fermi edge of the Ta sample holder. The spectrum of the Si(111)7 \times 7 surface shows the occupied surface states S_1 and S_2 at 0.2 and 0.9 eV, respectively. We cannot see the S_3 state clearly because of the projected bulk bands which hide it at this emission angle. The S_1 state seems to be crossing the Fermi level. The spectrum of the Si(111)3 \times 1-K surface shows a shoulder at 0.95 eV (S_2') and a peak at 1.6 eV (S_3'), but it shows no peak at the position of the S_1 state. These results suggest the disappearance of the Fermi-level crossing.

The ARUPS spectra of the Si(111)3 \times 1-K surface measured along the [11 $\bar{2}$] and [10 $\bar{1}$] directions are shown in Figs. 2(a) and 2(b), respectively. The accurate [11 $\bar{2}$] azimuthal direction was determined by measuring the symmetry of the dispersion around the observed symmetry point \bar{M} . The [10 $\bar{1}$] direction was set by rotating the sample azimuth by 30° from the [11 $\bar{2}$] direction. The ARUPS measurements were done at every 2° from $\theta_e=0^\circ$ to 18° and at every 3° from $\theta_e=18^\circ$ to 69° for the [11 $\bar{2}$] direction. For the [10 $\bar{1}$] direction, we measured the spec-

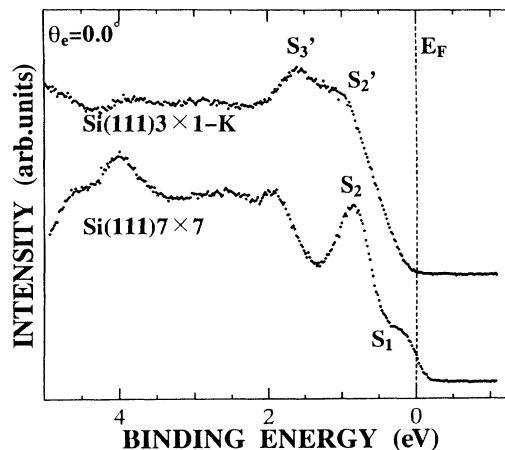


FIG. 1. Ultraviolet photoemission spectra of the Si(111)7 \times 7 clean surface and the Si(111)3 \times 1-K surface at emission angle $\theta_e=0^\circ$ for the photon energy of $h\nu=21.2$ eV.

tra at every 2° from $\theta_e = 0^\circ$ to 18° , at every 3° from $\theta_e = 18^\circ$ to 48° , and at every 4° from $\theta_e = 48^\circ$ to 76° . For both directions, the incidence angle of the photon, θ_i , is 45° from the surface normal for the region of θ_e from 0° to 39° , and $\theta_i = 35^\circ$ for $\theta_e > 39^\circ$. This change of θ_i was made so as to avoid the reflected light from entering the analyzer. Any spectrum in Figs. 2(a) and 2(b) does not show appreciable intensity at the Fermi level. In addition, no structure is observed near the E_B of the S_1 state. From these results, it is concluded that the Si(111)3×1-K surface is no longer metallic but semiconducting, and the Si dangling bonds are completely filled on this surface. By increasing the binding energy, we observed structures

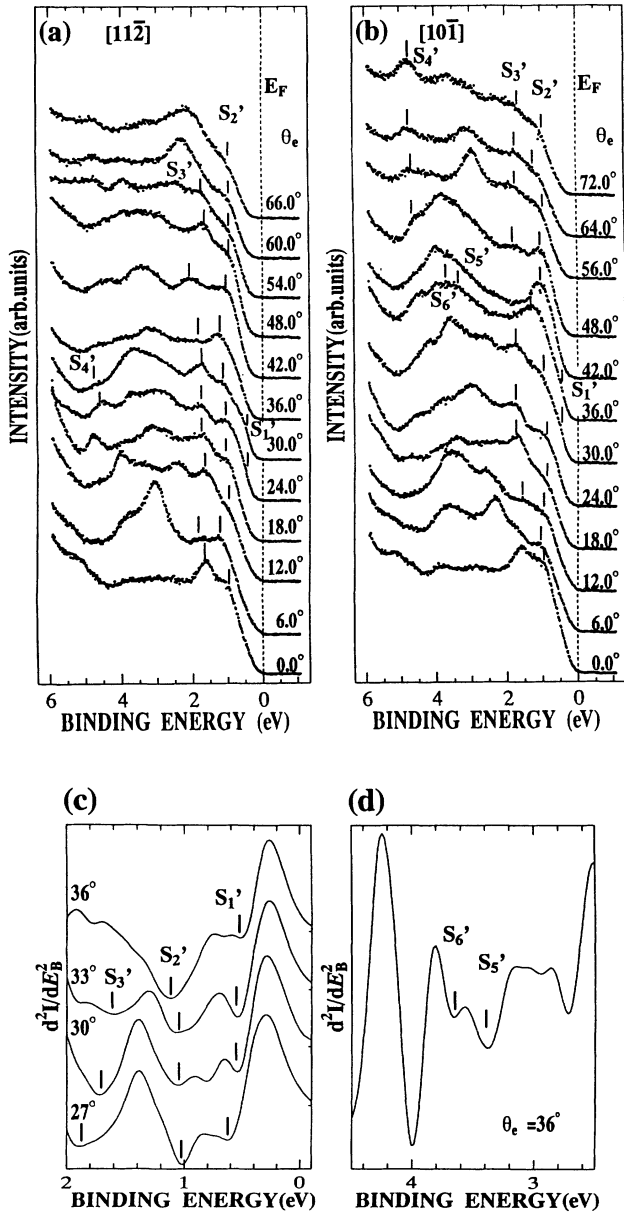


FIG. 2. ARUPS spectra of the Si(111)3×1-K surface along the (a) $[11\bar{2}]$ and (b) $[10\bar{1}]$ -directions. (c) The second derivative spectra at $\theta_e = 27^\circ, 30^\circ, 33^\circ$, and 36° , and (d) that at $\theta_e = 36^\circ$, for the $[10\bar{1}]$ direction. Tic marks indicate the surface-state's peaks (or the position of the minima of the second derivative spectra).

S'_1 (very weak shoulder), S'_2, S'_3, S'_4, S'_5 , and S'_6 as recognized in Figs. 2(a) and 2(b). These structures are in the band-gap region of the projected density of states as shown in Fig. 4 later. Figure 2(c) shows the second derivative spectra at $\theta_e = 27^\circ, 30^\circ, 33^\circ$, and 36° , for the $[10\bar{1}]$ direction. In this figure we can see the S'_1 state, which is difficult to confirm in both Figs. 2(a) and 2(b). Figure 2(d) shows the second derivative spectrum at $\theta_e = 36^\circ$ for the $[10\bar{1}]$ direction to clarify the S'_5 and S'_6 states.

We show in Fig. 3(a) the surface Brillouin zones of the Si(111)1×1 and the Si(111)3×1-K surface. The symbol $\bar{\Gamma}$ is the symmetry point of the 1×1 and the 3×1 surfaces and the symbols \bar{M} and \bar{K} are the symmetry points of the 1×1 surface. The symbols $\bar{A}, \bar{B}, \bar{C}, \bar{D}, \bar{E}, \bar{F}, \bar{G}$, and \bar{H} are used tentatively in this paper for describing the symmetry points shown in Fig. 3(a) in the 3×1 Brillouin zone. According to the threefold symmetry of the Si(111)1×1 surface structure, this 3×1 structure is composed of three sets of domains which differ by 120° in the azimuthal direction from each other. Hence, we must consider three types of the surface Brillouin zones of the 3×1 structure as shown in Fig. 3(b). When we measure the ARUPS along the $[11\bar{2}]$ direction, we probe not only the information along the $\bar{\Gamma} \rightarrow \bar{C} \rightarrow \bar{\Gamma} \rightarrow \bar{C} \rightarrow \bar{\Gamma} \rightarrow \bar{C} \rightarrow \bar{\Gamma}$ direction but also that along the $\bar{\Gamma} \rightarrow \bar{E} \rightarrow \bar{F} \rightarrow \bar{E} \rightarrow \bar{\Gamma}$ direction. In the case for the $[10\bar{1}]$ direction, we likewise get information along the $\bar{\Gamma} \rightarrow \bar{G} \rightarrow \bar{H} \rightarrow \bar{A} \rightarrow \bar{B} \rightarrow \bar{E} \rightarrow \bar{D} \rightarrow \bar{C} \rightarrow \bar{D} \rightarrow \bar{E} \rightarrow \bar{A} \rightarrow \bar{B} \rightarrow \bar{H} \rightarrow \bar{G} \rightarrow \bar{\Gamma}$ direction in addition to that along the $\bar{\Gamma} \rightarrow \bar{D} \rightarrow \bar{G} \rightarrow \bar{E} \rightarrow \bar{H} \rightarrow \bar{F} \rightarrow \bar{H} \rightarrow \bar{E} \rightarrow \bar{G} \rightarrow \bar{D} \rightarrow \bar{\Gamma}$ direction at the same time.

Figure 4 summarizes the dispersion of the electronic states of the Si(111)3×1-K surface estimated from the present experiment. The filled circles represent the positions of the observed peaks and shoulders in the ARUPS spectra (or the positions of the minima of the second

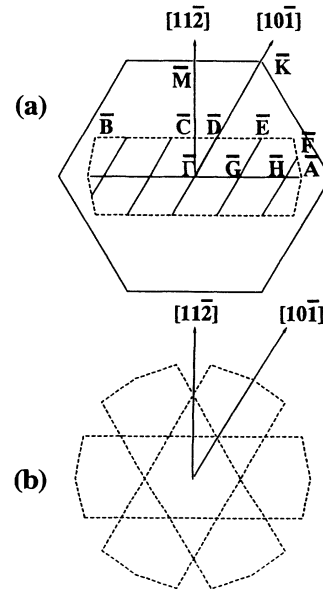


FIG. 3. (a) The surface Brillouin zones of the Si(111)1×1 and the Si(111)3×1-K surface. (b) The three equivalent 3×1 surface Brillouin zones.

derivative spectra). Their size represents the intensity of the peaks and shoulders classified visually. The open circles are the data reversed at the symmetry point \bar{M} . The projected bulk bands (hatched regions) are from Ref. 21. In the $[10\bar{1}]$ direction [Fig. 4(b)], the symmetry point \bar{K} of the 1×1 surface Brillouin zone corresponds only to the \bar{E} point of the 3×1 surface Brillouin zone. Regarding this symmetry point, we can see five surface states ($S'_1, S'_2, S'_3, S'_5,$ and S'_6 at 0.54, 1.07, 1.59, 3.39, and 3.67 eV, respectively) in the band gap. In addition, we can recognize one more surface state near the \bar{M} point, in the gap at about 4.75 eV. Therefore, the number of surface states will be six. But we do not discuss the surface states (S'_5 and S'_6) near the \bar{K} point of the 1×1 surface Brillouin zone because the number of data points were limited. Since we have substantially probed the two directions in the 3×1 Brillouin zone at the same time, we expect seven structures of the surface states for four surface-state branches, which we can guess from the above dis-

cussion. These seven surface-state structures are indicated in Fig. 5 by crosses for S'_1 , solid lines for $S'_{2A}, S'_{3A},$ and S'_{4A} , and by broken lines for $S'_{2B}, S'_{3B},$ and S'_{4B} (where the broken line is hidden by the filled circles). The solid and broken lines correspond to the dispersion of the surface states along the $\bar{\Gamma}\rightarrow\bar{C}\rightarrow\bar{\Gamma}\rightarrow\bar{C}\rightarrow\bar{\Gamma}\rightarrow\bar{C}\rightarrow\bar{\Gamma}$ and $\bar{\Gamma}\rightarrow\bar{E}\rightarrow\bar{F}\rightarrow\bar{E}\rightarrow\bar{\Gamma}$ for the $[11\bar{2}]$ direction in Fig. 5(a), and along the $\bar{\Gamma}\rightarrow\bar{G}\rightarrow\bar{H}\rightarrow\bar{A}\bar{B}\rightarrow\bar{E}\rightarrow\bar{D}\rightarrow\bar{C}\rightarrow\bar{D}\rightarrow\bar{E}\rightarrow\bar{A}\bar{B}\rightarrow\bar{H}\rightarrow\bar{G}\rightarrow\bar{\Gamma}$ and $\bar{\Gamma}\rightarrow\bar{D}\rightarrow\bar{G}\rightarrow\bar{E}\rightarrow\bar{H}\rightarrow\bar{F}\rightarrow\bar{H}\rightarrow\bar{E}\rightarrow\bar{G}\rightarrow\bar{D}\rightarrow\bar{\Gamma}$ for the $[10\bar{1}]$ direction in Fig. 5(b). The surface-state bands $S'_{2A}, S'_{2B}, S'_{3A}, S'_{3B}, S'_{4A},$ and S'_{4B} are traced by considering the equivalence of E_B at each symmetry point. For example, the E_B at one symmetry point \bar{C} is equivalent to another \bar{C} point along each direction. Likewise the E_B at the symmetry point \bar{G} is equivalent at the other \bar{G} point along the $\bar{\Gamma}\rightarrow\bar{G}\rightarrow\bar{H}\rightarrow\bar{A}\bar{B}\rightarrow\bar{E}\rightarrow\bar{D}\rightarrow\bar{C}\rightarrow\bar{D}\rightarrow\bar{E}\rightarrow\bar{A}\bar{B}\rightarrow\bar{H}\rightarrow\bar{G}\rightarrow\bar{\Gamma}$

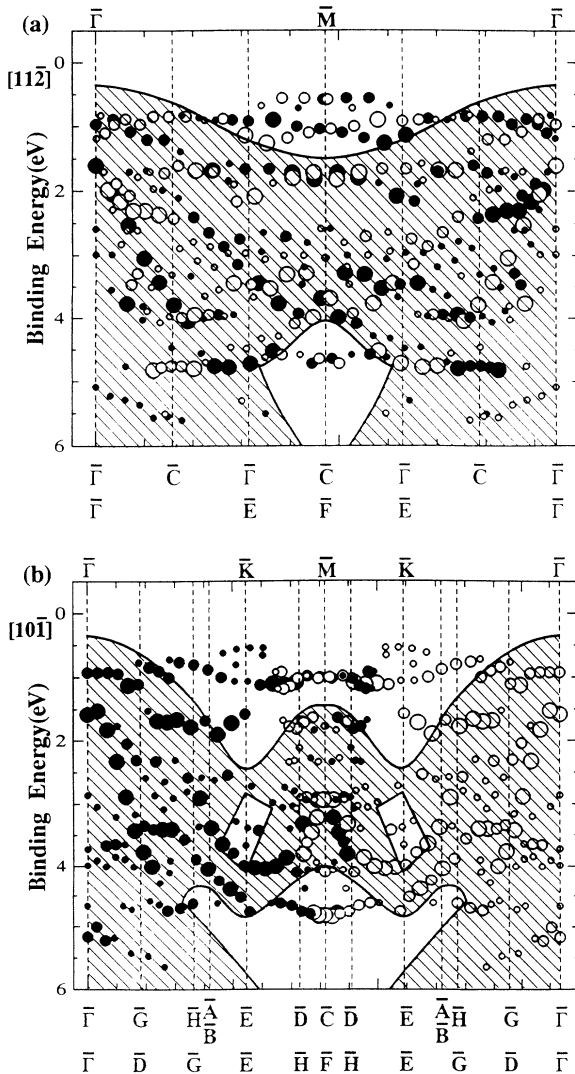


FIG. 4. Dispersion of the electronic states of the Si(111) 3×1 -K surface along the (a) $[11\bar{2}]$ and (b) $[10\bar{1}]$ directions. The hatched area represents the projected bulk states.

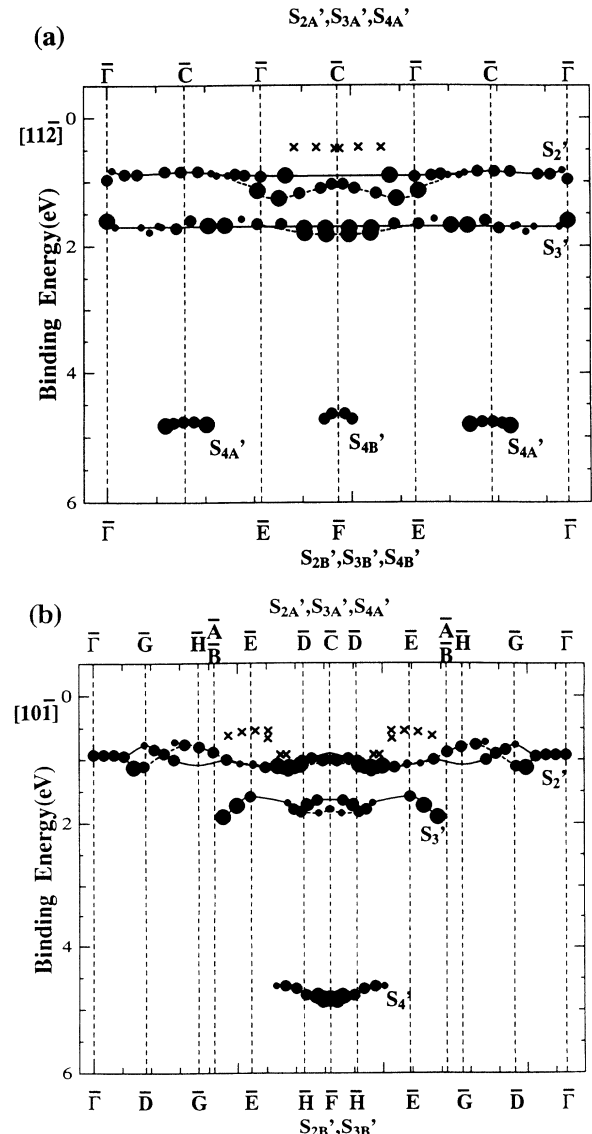


FIG. 5. Dispersion of the surface states along the (a) $[11\bar{2}]$ and (b) $[10\bar{1}]$ directions.

$\bar{\Gamma} \rightarrow \bar{D} \rightarrow \bar{G} \rightarrow \bar{E} \rightarrow \bar{H} \rightarrow \bar{F} \rightarrow \bar{H} \rightarrow \bar{E} \rightarrow \bar{G} \rightarrow \bar{D} \rightarrow \bar{\Gamma}$, respectively. For S'_{2A} , S'_{2B} , and S'_{3A} the width of the dispersion is thus ~ 0 , ~ 0.35 , and ~ 0 eV along the $[11\bar{2}]$ direction and ~ 0.42 , ~ 0.47 , and ~ 0.32 eV along the $[10\bar{1}]$ direction, respectively. We cannot estimate the width of the dispersion of S'_{3B} , S'_{4A} , and S'_{4B} because of the scarcity of data as a result of an appreciable overlap with the bulk bands.

We then compare the present result with the surface state of the Si(111)2×1 clean surface. The smallest E_B of the S'_1 state is found near the \bar{F} point in Fig. 5(a) (this point is not considered to be the \bar{C} point because of a comparison with the result on the 3×1-Na surface²²) or \bar{E} point in Fig. 5(b). We consider that the S'_1 state is degenerated with the S'_2 state at the $\bar{\Gamma}$ point ($E_B \approx 0.9$ eV), because there is no other surface peak near this energy. The angular dispersion shown in Fig. 2(c) supports this assumption, because the S'_1 state shifts to larger E_B with decreasing θ_e below 30°. Therefore, it is strongly suggested that the S'_1 state has a positive dispersion parallel to the chains, going from $\bar{\Gamma}$ to \bar{K} of the 1×1 surface Brillouin zone. The difference of E_B between the $\bar{\Gamma}$ point and the \bar{F} point, which is on the way between the \bar{J} and \bar{K}' points in the 2×1 surface Brillouin zone, becomes ~ 0.48 eV in qualitative agreement with the above estimation. In the next place, the results of the dispersion along the $\bar{\Gamma}-\bar{J}'$ direction are much different between Pandey and Northrup and Cohen. The width calculated by Pandey is almost 0 eV, whereas the result of Northrup and Cohen's is 0.37 eV with the smallest E_B at the $\bar{\Gamma}$ point. We could not see any dispersion along the $\bar{\Gamma}-\bar{C}$ direction, which is the direction corresponding to their $\bar{\Gamma}-\bar{J}'$ direction. Thus our result is consistent with that of Pandey. Considering the similarity in the width of the dispersion (although we estimated only by the difference of E_B between the $\bar{\Gamma}$ and \bar{E} points for the $[10\bar{1}]$ direction), which reflects the overlap of the involved wave function, as well as in the behavior of the dispersion along the equivalent directions of the 3×1 and 2×1 surface Brillouin zones, the data points denoted by crosses in Fig. 5 are assigned to a part of the surface state derived from the π -bonded chain (S'_1 state). It is not unrealistic that the Si(111)3×1-K surface contains the reconstructed π -bonded chain.

Since the S'_1 state is found at 0.5 eV below the Fermi level, the surface-state band gap will be larger than 0.5 eV. On the Si(111)3×1-Na surface the S'_1 state is located at about 0.8 eV below the Fermi level²² and it was shown that the surface-state band gap of this Na-covered surface is ≈ 1 eV by STS.¹³ These band gaps are appreciably larger than the value of 0.25 eV calculated by Pandey¹⁸ for the Si(111)2×1 surface. But the experimentally reported values 0.45 (Ref. 23) and 0.47 eV,²⁴ for the Si(111)2×1 surface, are comparable with the present evaluation. The difference between the Si(111)2×1 and Si(111)3×1-(K,Na) surfaces may be due to the effect of the alkali metal, or to the different structural relaxation or distortion.

Figure 6 summarizes the results of dispersion along the boundary of the 3×1 surface Brillouin zone, i.e., for $\bar{\Gamma} \rightarrow \bar{G} \rightarrow \bar{H} \rightarrow \bar{A} \rightarrow \bar{F} \rightarrow \bar{B} \rightarrow \bar{E} \rightarrow \bar{D} \rightarrow \bar{C} \rightarrow \bar{\Gamma}$, from which

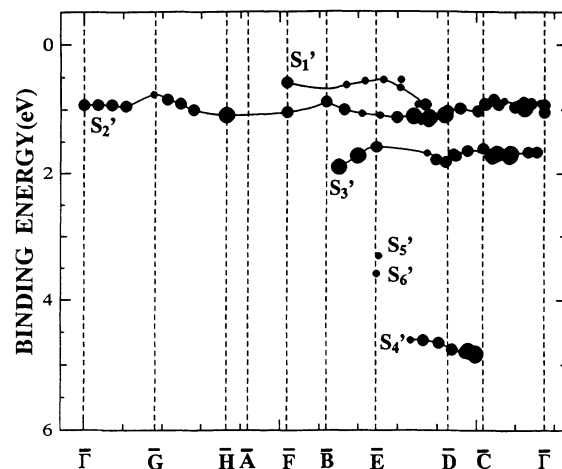


FIG. 6. Dispersion along the boundary of the 3×1 surface Brillouin zone.

the width of the dispersion of the Si(111)3×1-K surface is estimated as ~ 0.48 eV for the S'_1 state, ~ 0.47 eV for the S'_2 state, and ~ 0.32 eV for the S'_3 state. In this figure, we can see clearly four surface-state branches and two other surface states.

XPS results are summarized in Table I. The peak intensities of the Si L_{VV} Auger and the K $2p$ core emission as well as their ratio for the Si(111)87×7-K and Si(111)3×1-K surfaces are tabulated. It should be remembered that these surfaces correspond to the saturation coverage at room temperature and at around 500°C. From this table, the saturation coverage of Si(111)3×1-K is determined to be 0.33 times that of the saturation coverage at room temperature. Daimon and Ino considered the saturation coverage of the Si(111)87×7-K as 1 ML.⁵ The atomic radius of the adsorbed K atoms (which is partially ionized) is considered to be smaller than that in the metallic phase (2.3 Å) and larger than that of K^+ (1.3 Å). There is also a fact that K atoms on the Si(001)2×1-K surface stack with the Si-Si distance of 3.84 Å.²⁵ The half of the nearest-neighbor distance of the Si atoms ($3.84 \text{ Å}/2 = 1.92 \text{ Å}$) is the same on both the (001) and (111) surfaces. The atomic radius of the adsorbed K, which is partly ionized, is considered to be comparable to or smaller than this value (1.92 Å), and the K saturation coverage of 1 ML on the Si(111)87×7-K is not unrealistic. On the other hand, the photoemission data in Ref. 16 have suggested one K atom per Si dangling bond, i.e., the saturation coverage as $\frac{19}{49} \approx 0.4$ ML, for the Si(111)87×7-K surface. Then we think the lower limit of the saturation coverage of the Si(111)3×1-K surface as 0.13 ML

TABLE I. Intensities of Si L_{VV} Auger and K $2p$ and their intensity ratios (K/Si) measured by XPS.

	87×7	3×1
Si L_{VV} Auger	1470	1640
K $2p$	158.6	59
K/Si	0.1079	0.036

($\frac{19}{49} \times \frac{1}{3}$) and the upper limit as $\frac{1}{3}$ ML, and the number of K atoms in the 3×1 unit mesh of the 3×1 structure will be between 0.4 and 1. Considering these limits, we prefer the saturation coverage of $\frac{1}{3}$ ML, because the number of K atoms in the 3×1 unit mesh should naturally be an integer when the alkali metals are perfectly ordered. This result is consistent with the recent ISS result of Hashizume *et al.*⁷ However, this value is much different from that estimated by RHEED (Ref. 5) or those of STM,^{6,12,13} which proposed the saturation coverage of $\frac{2}{3}$ ML. This difference might be caused by the sample temperature of those experiments not being high enough, and the structures not being completely 3×1 , and a mixture of the $\delta 7 \times 7$ surface leads to the coverage larger than ours. As for the STM image, we will argue it later. Besides, the value reported by Fan and Ignatiev¹¹ (0.01 ML) is much smaller than ours. This difference may be caused by the difference of the sample preparation method of the 3×1 surface. That is, they first exposed the surface to the alkali metal at room temperature and then annealed it at higher temperature (about 800°C) to make a 3×1 structure. In this method, most of the alkali-metal atoms might have desorbed and the coverage might have become much less than ours.

From the present results, we propose a structural model for the Si(111) 3×1 -K surface as shown in Fig. 7 in which (a) shows the side view and (b) shows the top view of this surface. The large and small dotted circles represent the positions of the first-layer and the second-layer Si atoms of the Si(111) 1×1 ideal surface, respectively. The shaded circles represent the Si atoms which constitute the π -bonded chain and the large filled circles represent the K atoms. The thick lines represent the unit mesh of the 3×1 structure. This model is similar to that proposed by Wan, Lin, and Nogami,¹² but there are two different points. First, the number of alkali metals in the unit cell is not two but one, suggesting the clear difference of the saturation coverage. Second, in the model of Wan, Lin, and Nogami, the dangling bonds of the “ π -bond-like” Si atoms are terminated by the Li atoms. But in our model they are not terminated by alkali metals, and these dangling bonds make the π -bonded

chain like the Si(111) 2×1 surface. The present model can explain the result of the STM experiment^{6,12,13} from a different standpoint. Namely, the filled electronic state probed by the STM is not due to the K atoms but due to the dangling bonds of the π -bonded chain Si atoms in accord with the zigzag image of the STM, and the empty state is not resulting from the Si atoms but from the K atoms. This model has a good agreement with the result of LEED,^{9–11} i.e., not only the K atoms but the Si atoms make a 3×1 structure. Considering the difference between the direction of the dangling bonds of the five-membered rings and that of the seven-membered rings, the dispersion of the present π -bond surface state should be much smaller than that of the Si(111) 2×1 surface, because the dangling bonds on the five-membered rings are tilted compared with those of the seven-membered rings in which they are nearly parallel. Although this is an unsolved problem, this model still seems reasonable allowing interpretation of the previous STM data.^{6,12,13} But we have to mention that some kind of structural relaxation or distortion is probably needed to open a large band gap. Therefore, we think that this model is only tentative and more structural data and/or theoretical works are needed.

According to this model, the number of the clear surface states will be at least four: (a) surface state of the π bond, (b) that of the Si-K bonding, (c) that of the σ bond among the π -bonded chain Si atoms, and (d) that of the σ bond between the first-layer Si atoms and the π -bonded chain Si atoms. Judging from the similarity of the dispersion as discussed above, the S'_1 state is assigned to (a). The UPS spectra measured by Tezuka, Daimon, and Ino¹⁷ and Magnusson and Reihl¹⁶ have a surface state at ~ 1 eV below the Fermi level. Considering the similarity of E_B and the structure of Si-K bonding [on-top site for the Si(111) $\delta 7 \times 7$ -K surface], the S'_2 state is assigned to (b). Himpsel, Heimann, and Eastman²⁶ observed three surface states on the Si(111) 2×1 surface. One will be the surface state of the π bond and the others the surface states that are caused by the π -bonded chain, that is (c) and (d). We only have a little information about the S'_3 and S'_4 states, but according to the result of Himpsel, Heimann, and Eastman,²⁶ these surface states could be (c) and (d).

Figure 8 shows the change of the work function against the deposition time of K for the Si(111) $\delta 7 \times 7$ -K surface at room temperature. The work function of the Si(111) 3×1 -K is also shown by an open circle at its deposition time at 500°C. We have to pay attention to the difference of the sticking coefficient at different temperatures (room temperature and 500°C). The reduction of the work function of the surface for the saturation coverage is 2.95 eV (which is almost the same as that of Ref. 16) for the Si(111) $\delta 7 \times 7$ -K surface and 1.37 eV for the Si(111) 3×1 -K surface. We conclude that a saturated monolayer for the Si(111) $\delta 7 \times 7$ -K is formed after 5.5 min under this deposition condition. The saturation coverage of the Si(111) 3×1 -K surface is formed after 3.5 min of K deposition. One should also be reminded of the temperature difference of the Si substrate. The deposition time for the saturation coverage of the Si(111) 3×1 -K surface

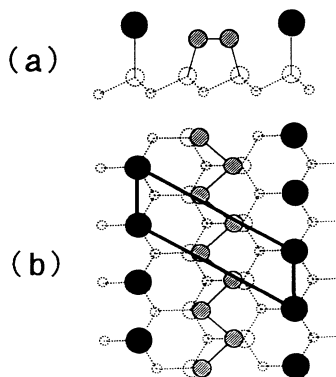


FIG. 7. Structural model for the Si(111) 3×1 -K surface, (a) side view and (b) top view.

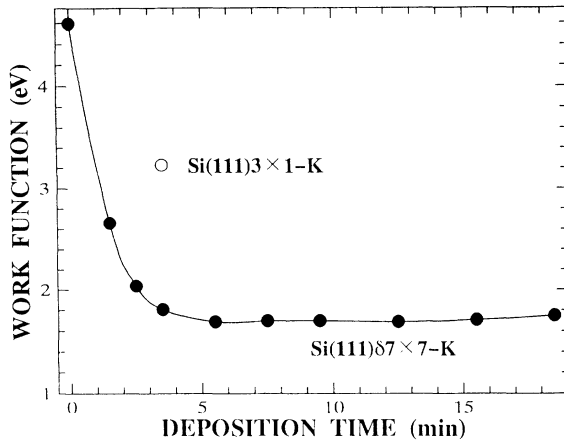


FIG. 8. Change of the work function against the deposition time for the Si(111)87×7-K and the Si(111)3×1-K surface.

is not $\frac{1}{3}$ of the Si(111)87×7-K because the K atoms not only adsorb on the Si surface but also desorb from it at 500°C. It might be simply thought that the change of the work function of the Si(111)3×1-K surface will be $\frac{1}{3}$ of that of the Si(111)87×7-K surface in contrast to our present result. But, since the work function changes radically in the early stage of adsorption and the change becomes less with increasing the K adsorption due to the dipole-dipole interaction, we have to compare the change of work function for the Si(111)3×1-K surface to that for the Si(111)87×7-K surface at $\frac{1}{3}$ ML, i.e., compare the change at the same coverage. The work-function change of the Si(111)3×1-K surface is smaller than that of the Si(111)87×7-K surface at the deposition time corresponding to $\frac{1}{3}$ of the saturation value. This small work-function change of the Si(111)3×1-K surface compared with the $\frac{1}{3}$ ML Si(111)87×7-K surface can also be explained by our model. Looking at Fig. 7(a), we recognize that the interlayer distance between the layer of K atoms and that of π -bonded chain Si atoms is very short. Hence, the dipole moment between the K layer and the Si layer must be small. On the other hand, K atoms are thought to be adsorbed at the on-top site on the Si(111)87×7-K surface. Therefore, the work-function change should be larger than that of the Si(111)3×1-K surface because of the larger interlayer distance and larger dipole moment.

In this model for the Si(111)3×1-K surface, no dangling bond remains and the surface should not be metallic but semiconducting. Therefore, this surface structural model is consistent with the semiconducting surface electronic state. Our results of the Si 2*p* core-level shift for the Si(111)3×1-Na surface¹⁴ also support these results.

SUMMARY

The surface electronic states and the saturation coverage of the Si(111)3×1-K surface are studied using not only angle-resolved ultraviolet photoelectron spectroscopy but also x-ray photoelectron spectroscopy. It is found for the Si(111)3×1-K that the S_1 state of the Si(111)7×7 clean surface at ~ 0.2 eV below the Fermi level disappears and surface states S'_2 and S'_3 appear at 0.95 and 1.6 eV below the Fermi level, with no Fermi-level crossing. So, the Si(111)3×1-K surface is no longer a metallic surface such as the Si(111)7×7 clean surface but a semiconducting surface. We measured the dispersion along the [11 $\bar{2}$] and [10 $\bar{1}$] directions and found other surface states, S'_1 and S'_4 . We discussed these surface states in this paper. The other surface states observed at 3.39 and 3.67 eV below the Fermi level are not discussed here. The widths of the band dispersions are ~ 0.48 eV for the S'_1 state, ~ 0.47 eV for the S'_2 state, and ~ 0.32 eV for the S'_3 state. We cannot evaluate the width of the dispersion of the S'_4 state because of the scarcity of data. Judging from the dispersion behavior, the S'_1 and S'_2 states have been assigned to the surface state of the π bond and that of the Si-K bonding, respectively. Taking into account the results of other experiments, the S'_3 and S'_4 states might be assigned to the σ bond among the π -bonded chain Si atoms and that of the σ bond between the first-layer Si atoms and the π -bonded chain Si atoms, respectively.

The saturation coverage of the Si(111)3×1-K surface was estimated to be $\frac{1}{3}$ ML from a comparison of the Si Auger and the K 2*p* photoemission intensity ratio with that of the Si(111)87×7-K surface on which the saturation coverage is thought to be 1 ML.

Based on these results we have proposed a model of the Si(111)3×1-K surface. This model can explain the semiconducting surface electronic state, STM image, the smaller work-function change compared with that of the Si(111)87×7-K surface, as well as the dispersion and the number of surface states.

ACKNOWLEDGMENTS

The authors are grateful to Professor K. Cho, Professor K. Makoshi, and Dr. T. Ohfuchi of Osaka University for their critical discussions. They also acknowledge the staff and graduate students of SRL, ISSP, and the University of Tokyo for their hospitality during the experiment. Part of this study was supported by a Grant-in-Aid for Scientific Research from the Ministry of Education, Science and Culture.

¹H. Tochiyara, Surf. Sci. **126**, 523 (1983).

²T. Aruga, H. Tochiyara, and Y. Murata, Phys. Rev. Lett. **33**, 372 (1984).

³Y. Enta, T. Kinoshita, S. Suzuki, and S. Kono, Phys. Rev. B **36**, 9801 (1987).

⁴Y. Enta, T. Kinoshita, S. Suzuki, and S. Kono, Phys. Rev. B **39**, 1125 (1989).

⁵H. Daimon and S. Ino, Surf. Sci. **164**, 320 (1985).

⁶T. Hashizume, Y. Hasegawa, I. Sumita, and T. Sakurai, Surf. Sci. **246**, 189 (1991).

- ⁷T. Hashizume, M. Katayama, D. Jeon, M. Aono, and T. Sakurai, *Jpn. J. Appl. Phys.* **32**, L1263 (1993).
- ⁸S. Mizuno and A. Ichimiya, *Appl. Surf. Sci.* **33/34**, 38 (1988).
- ⁹W. C. Fan and A. Ignatiev, *Phys. Rev. B* **40**, 5479 (1989).
- ¹⁰J. Quinn and F. Jona, *Surf. Sci. Lett.* **249**, L307 (1991).
- ¹¹W. C. Fan and A. Ignatiev, *Phys. Rev. B* **41**, 3592 (1990).
- ¹²K. J. Wan, X. F. Lin, and J. Nogami, *Phys. Rev. B* **46**, 13 635 (1992).
- ¹³D. Jeon, T. Hashizume, T. Sakurai, and R. F. Willis, *Phys. Rev. Lett.* **69**, 1419 (1992).
- ¹⁴T. Okuda, H. Shigeoka, D. Daimon, S. Suga, T. Kinoshita, and A. Kakizaki (unpublished).
- ¹⁵U. A. Ditzinger, Ch. Lunau, B. Schieweck, St. Tosch, and H. Neddermeyer, *Surf. Sci.* **211/212**, 707 (1989).
- ¹⁶K. O. Magnusson and B. Reihl, *Phys. Rev. B* **41**, 12 071 (1990).
- ¹⁷Y. Tezuka, H. Daimon, and S. Ino, *Jpn. J. Appl. Phys.* **29**, 1773 (1990).
- ¹⁸K. C. Pandey, *Phys. Rev. Lett.* **47**, 1913 (1981).
- ¹⁹R. I. G. Uhrberg, G. V. Hansson, J. M. Nicholls, and S. A. Flodstrom, *Phys. Rev. Lett.* **48**, 1032 (1982).
- ²⁰J. E. Northrup and M. L. Cohen, *Phys. Rev. Lett.* **49**, 1349 (1982).
- ²¹K. C. Pandey, *Phys. Rev. B* **14**, 1557 (1976).
- ²²T. Okuda, K. Sakamoto, N. Nishimoto, H. Daimon, S. Suga, T. Kinoshita, and A. Kakizaki (unpublished).
- ²³Per Mårtensson, A. Cricenti, and G. V. Hansson, *Phys. Rev. B* **32**, 6959 (1985).
- ²⁴M. A. Olmstead and N. M. Amer, *Phys. Rev. Lett.* **52**, 1148 (1984).
- ²⁵T. Abukawa and S. Kono, *Surf. Sci.* **214**, 141 (1989).
- ²⁶F. J. Himpsel, P. Heimann, and D. E. Eastman, *Phys. Rev. B* **24**, 2003 (1981).